19. Vorlesung

11. 7. 1991

# Einführung in die

# Nukleare Festkörperphysik

## Teil II./3.

SS 1991.

# Rutherford - Rückstreuung (RBS)

⇧

Rutherford backscattering

**Prinzip:** Energieverlust leichter Ionen an den Atomen der Probe.

**Energieverlust:**
- elastische Streuung an Atomkernen (kinematischer Energieverlust)
- inelastische Streuung an Elektronen (Bremsung)

Information aus elastische Streuung an Kernen:

Masse (chemische Analyse)

aus inelastische Streuung an Elektronen:

tiefenselektive Analyse

(Profilanalyse)

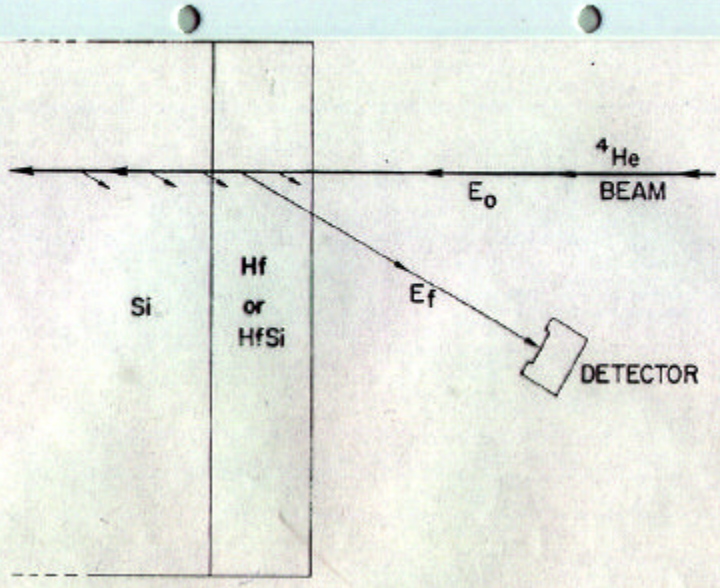


Figure 1) The basic experimental arrangement for nuclear backscattering is shown. The incident beam is usually $^1H^+$ (200-400 keV) or $^4He^+$ (1-3 MeV). Most of the beam penetrates deep into the sample. A few ions undergo a large-angle collision with target nuclei and come back out of the sample. They are detected by a surface-barrier detector, which also can determine each backscattered ion's energy to better than 1%. The target shown is a thin metal layer on a substrate of silicon. This target will be used for an example throughout this chapter.

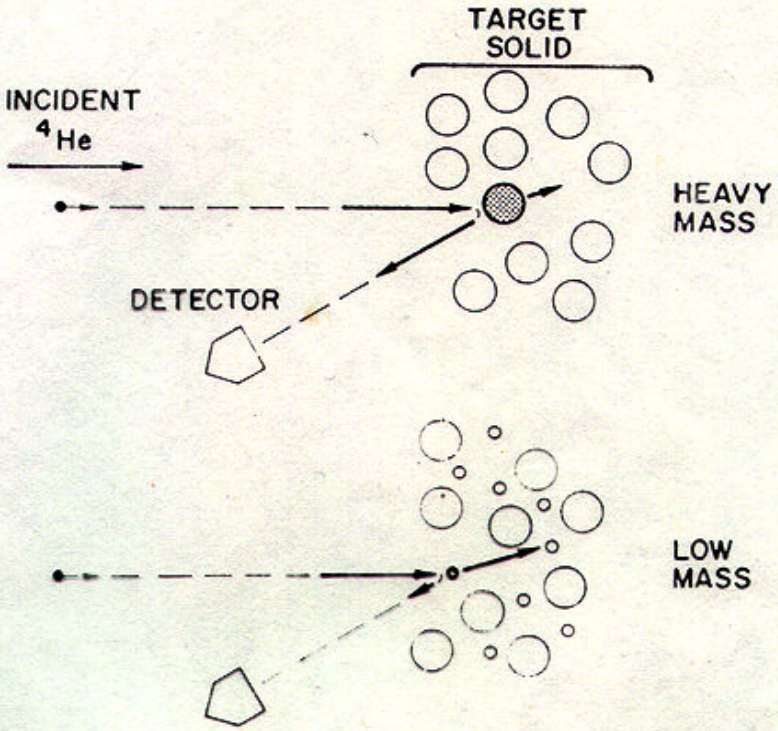


**Figure 2)** The primary effect in nuclear backscattering is conservation of momentum. This effect provides a correlation between the final backscattered ion energy and the mass of the target nucleus it hit. The upper drawing illustrates that if the ion hits a very heavy target nucleus, this nucleus will absorb little energy, and the backscattered ion will retain most of its original energy. In the lowest figure it is shown that if the ion backscatters from a light target nucleus, most of its energy will be transferred to that nucleus (to conserve momentum), and the backscattered ion will retain only a small part of its original energy.

# Apparatur

Beschleuniger (Van de Graaff o. Tandem)

Analysator-Magnet

Beam line und Kollimator

Goniometer und Probe

Energieempfindlicher Teilchendetektor

Verstärker

Vielkanalanalysator

Ionenstrom-Messung mit Integrator

Vakuumsystem

⋮

Ionensorten: $^4He^+$, $H^+$, $^{14}N^+$, $^{16}O^+$, $D^+$, ...

für spezielle Anwendungen

# Kinematischer Energieverlust

Elastischer Stoß: Energieerhaltung
Impulserhaltung

Energieverhältnis:

$$k = \frac{E_1}{E_0} = \left[ \frac{\sqrt{1 - \left(\frac{M_1}{M_2}\right)^2 \sin^2\theta} + \frac{M_1}{M_2}\cos\theta}{1 + \frac{M_1}{M_2}} \right]^2$$

$\theta$: Streuwinkel

$E_0$: Energie vorm Stoß

$E_1$: Energie nach dem Stoß

$M_1$: Masse des Ions

$M_2$: Masse des Target-Atoms

Für $\theta = \pi$:

$$k = \left(\frac{M_2 - M_1}{M_2 + M_1}\right)^2$$

| | C | N | O | Si | Au |
|---|---|---|---|---|---|
| $k^{170°}_{He}$ | 0.25 | 0.31 | 0.36 | 0.56 | 0.91 |

# Zählrate (Amplitude des Spektrums) und Wirkungsquerschnitt der Streuung

Differentielle Wirkungsquerschnitt der Rutherford-Streuung:

$$\frac{d\sigma}{d\Omega} = \left[\frac{Z_1 Z_2 e^2}{2E \sin^2\theta}\right]^2 \frac{\left[\cos\theta + \sqrt{1-\left(\frac{M_1}{M_2}\right)^2 \sin^2\theta}\,\right]^2}{\sqrt{1-\left(\frac{M_1}{M_2}\right)^2 \sin^2\theta}}$$

$E := E_0$ (i.a. Energie des einfallenden Ions bei der Streuung)

$Z_1, Z_2$: Ordnungszahlen ($\hat{=} M_1, M_2$)

Wirkungsquerschnitt nachgewiesen durch einen Detektor vom Raumwinkel $\Omega$:

$$\sigma = \frac{1}{\Omega} \int_{\Omega} \frac{d\sigma}{d\Omega}\, d\Omega$$

Spektrum-Amplitude:

$$A = \sigma\ \Omega\ Q\ N\ t$$

$N$: Konzentration, $t$: Dicke

$N\,t$: Flächendichte (Atom/cm²)

$Q$: Anzahl der einfallenden Teilchen

# Tiefenskala, elektronische Bremskraft

Energieverlust / Tiefe:

$$\frac{dE}{dx} = f(x, E, M_1, M_2)$$

$\Uparrow$

Tiefe

Bremswirkungsquerschnitt:

$$\varepsilon := \frac{1}{N} \frac{dE}{dx}$$

Die Teilchen werden von der Energie $E_0$ auf Energie $E$ abgebremst in der Tiefe

$$X = - \int_{E_0}^{E} \frac{dE}{\left(\frac{dE}{dx}\right)}$$

Näherung: die Bremskraft ist jeweils für eindringenden und für austretenden Ionen konstant:

$$\left.\frac{dE}{dx}\right|_{ein} \quad \text{und} \quad \left.\frac{dE}{dx}\right|_{aus}$$

Die eindringenden Ionen werden von der Energie $E_0$ auf Energie $E$ abgebremst:

$$E_0 - x \left.\frac{dE}{dx}\right|_{ein} = E$$

Rutherford-Streuung:

$$E \rightarrow kE$$

Energieverlust für auslaufenden Ionen:

$$kE - \frac{x}{\cos\theta} \left.\frac{dE}{dx}\right|_{aus} = E_1$$

$\Uparrow$

Bremsweg für unter Streuwinkel $\theta$ austretenden Ionen

Kante des Energiespektrums ($\hat{=}$ Energie der von der Oberfläche gestreuten Ionen): $kE_0$

Totaler Energieverlust:

$$\Delta E = kE_0 - E_1 =$$

$$= \left[ k \left.\frac{dE}{dx}\right|_{ein} + \frac{1}{\cos\theta} \left.\frac{dE}{dx}\right|_{aus} \right] x \approx$$

$$\approx \underbrace{\left[ k \left.\frac{dE}{dx}\right|_{E_0} + \frac{1}{\cos\theta} \left.\frac{dE}{dx}\right|_{kE_0} \right]}_{S} x$$

S (Energieverlustfaktor)

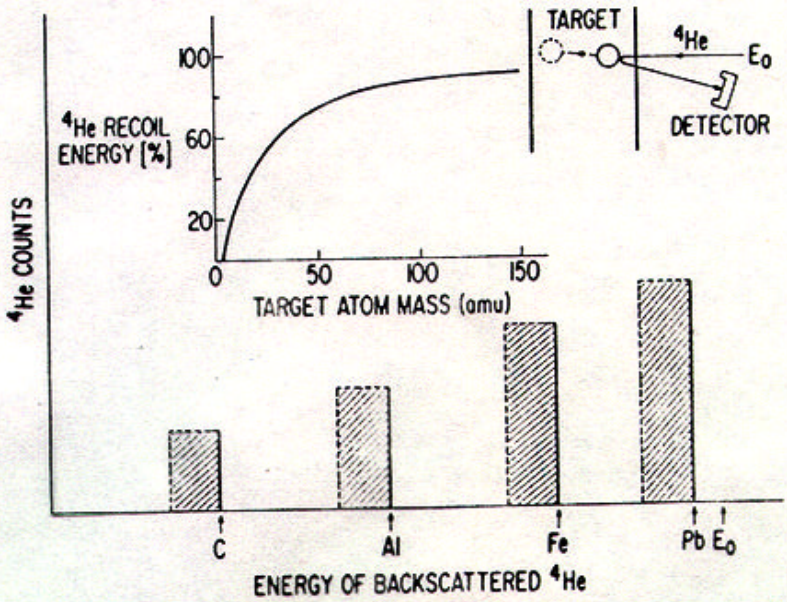


igure 3) The experimental arrangement of nuclear backscattering s shown in the upper right of the figure. Because of conservation f momentum the backscattered ion (the projectile ion is assumed to e $^4He^+$) will lose energy to the target nucleus it hits. The mount of energy retained by the backscattered ion varies with arget nuclear mass as shown in the upper left inset. The spectrum f final ion energies is shown in the bottom figure for various arget materials ($E_o$ is the original ion energy). As the ion pene- rates the film it loses small amounts of energy to the electron ea of the target. These small energy losses act to spread out ach film spectrum so that ions scattering from deeper in each film ppear as counts at slightly lower energy. Thus each peak directly ives a profile of target element concentration versus depth, with he surface being on the high energy side of each peak, and lower nergy counts coming from below the surface.

## Wie sollen RBS-Spektren gelesen werden?

- Große Änderungen der Energie ⇒ Masse des Target-Atoms
- Kleine Änderungen der Energie ⇒ Tiefe im Target
- Zählrate ⇒ $Z^2$ · Konzentration

  ⇓

  mehr empfindlich für schwere Elemente

Die Rutherford-Rückstreuung hat keine chemische Effekte, jedoch kann die Bildung einer Verbindung indirekt nachgewiesen werden.

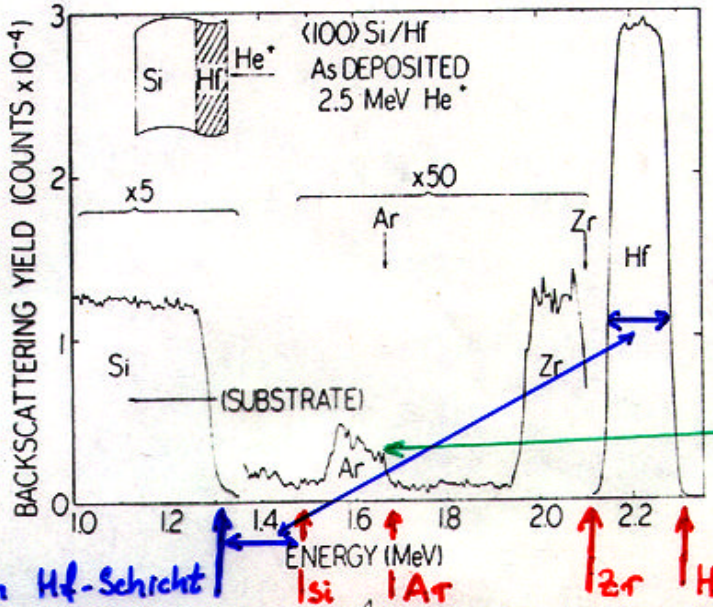


$^4He^+$ 2.5 MeV

10 Minuten

Konzentrations-profil für Ar.

Si unter dem Hf-Schicht | Si | Ar | Zr | Hf an der Oberfläche

**Figure 4)** Raw data is shown for $^4$He ion backscattering from a target of a metal film (Hf) on a Si substrate. The Hf peak occurs at high energy since $^4$He ions backscattering from Hf retains 91% of their original energy. This peak width indicates a Hf layer width of .16 μm. The peak is flat topped indicating a uniform layer. At lower energies there are two small peaks of Zr and Ar. The Zr is naturally present in Hf to about 3% since it can not be extracted chemically. The Ar is present because the Hf layer was sputtered and Ar was incorporated from the sputtering ambient. The tilt to the Ar peak indicates it is not uniform in the film. At the lowest energy in the figure is the Si substrate peak. This spectrum was accummulated in about 10 minutes.

0.15 μm Hf an Si

Zr: Verunreinigung in Hf

Ar: Aus Sputtering

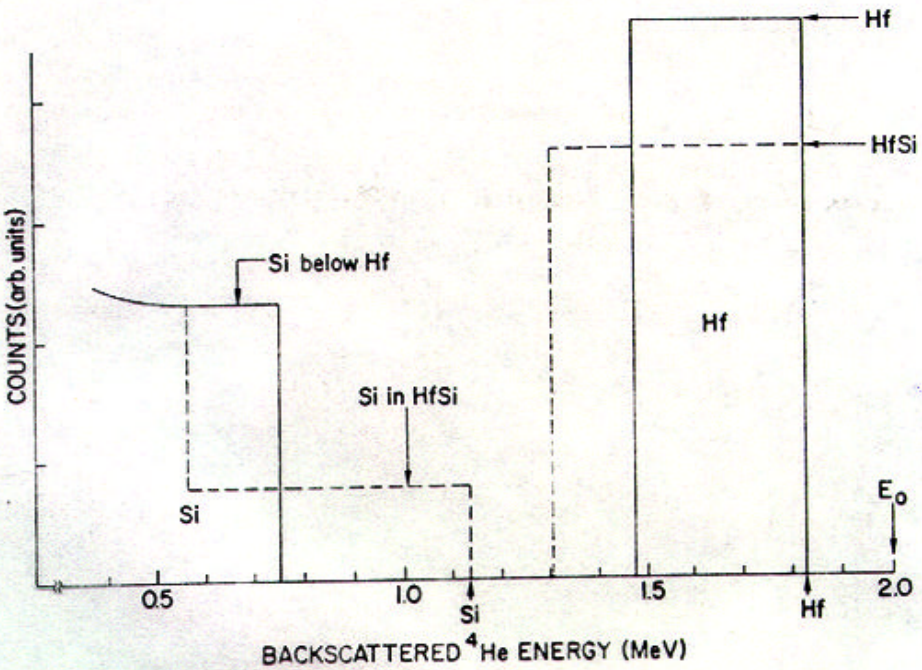


Figure 5) Simplified spectra are shown for Hf on Si (solid lines). and for HfSi on Si (dashed lines). The Hf peak changes with the formation of HfSi as the Hf is reduced in density by the Si, and the Hf layer becomes thicker. The Si substrate peak originally is displaced below its surface arrow because $^4$He ions must penetrate through the Hf film to reach the Si. The Si peak is offset to lower energy by about the width of the Hf peak. With the formation of HfSi, there is Si up to the Si surface arrow.

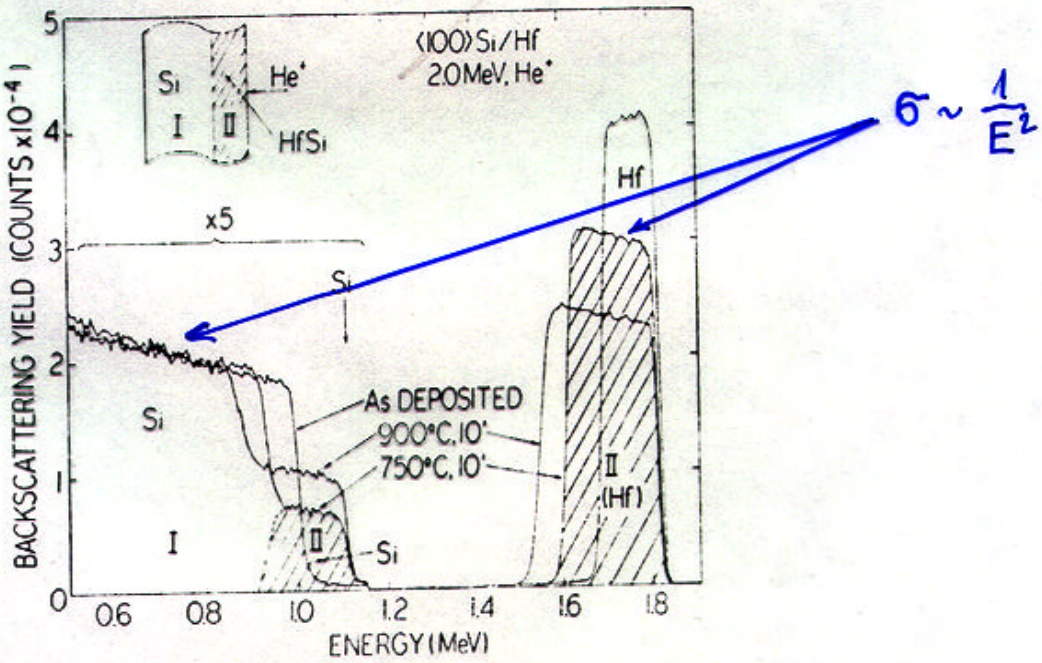


Figure 6) Raw data is shown for three superimposed spectra: Hf on Si; HfSi on Si; and $HfSi_2$ on Si. The Hf peak gets lower and wider as expected from the discussion of Figure 5. The original Si peak is displaced from the Si surface; but with the two silicides it is found at the surface. In each case, the experimental running time was 10 minutes.

Die Anzahl der Atome bleibt während der Festkörperreaktion konstant ⇒ die Flächen der entsprechenden Stpektrenteilen sind gleich.

- Das Bremsvermögen wird durch die mittlere Elektronendichte bestimmt ⇒ aus der chemischen Zusammensetzung kann das Bremsvermögen ⇒ Breite der Linie ⇒ Amplitude bestimmt werden.

- Diffusionsbegrenzte Reaktion kann auch im Zwischenzustand abgeschrecht werden ⇒ unvollständige Reaktion kann untersucht Werden.

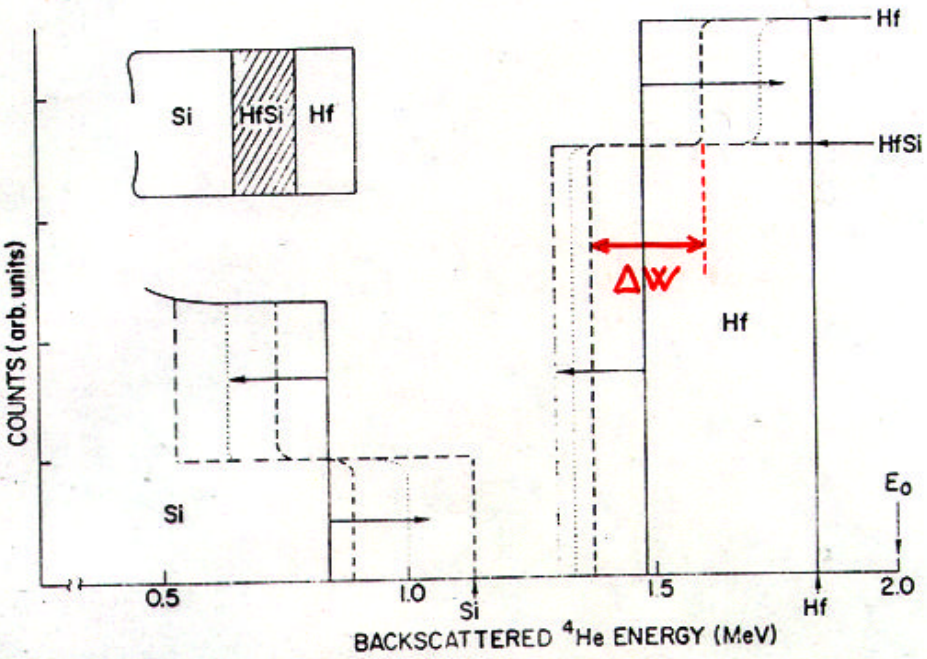


Figure 7) Simplified representation of spectra showing one formation process for HfSi. The upper left inset shows the assumption of HfSi formation at the interface of the Hf and Si materials. The HfSi layer expands as the formation continues, until the Hf is entirely converted. The Hf peak remains at full height near its surface energy, but at some depth it drops abruptly to the diluted level of Hf in HfSi. The Si substrate is originally lower than the Si surface energy because it is covered with Hf. As the HfSi formation process continues the Si extends out towards the Si surface.

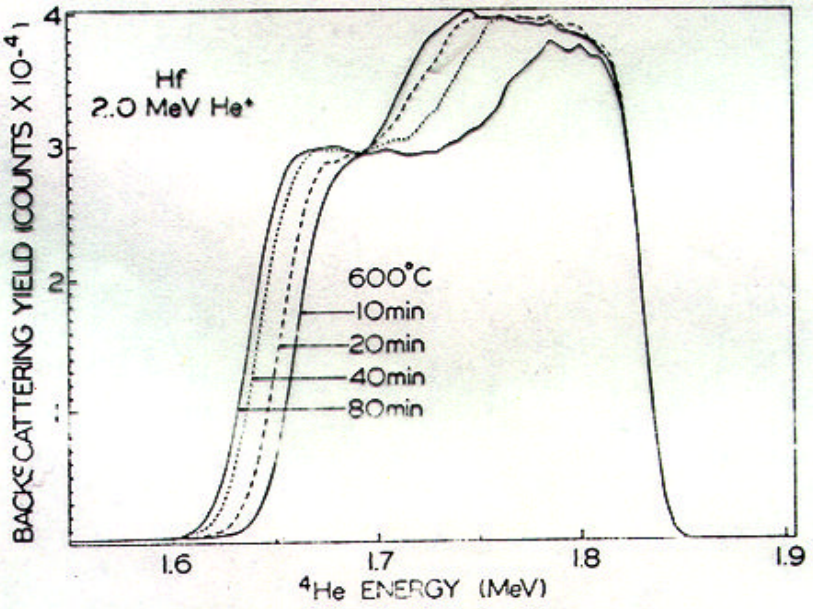


Figure 8) The raw data from the Hf portion of a series of spectra are shown. HfSi is first forming at the deepest part of the Hf layer, and this conversion of Hf to HfSi continues as the sample is heated for longer times. The energy width, ΔW, indicates the amount of HfSi formed.

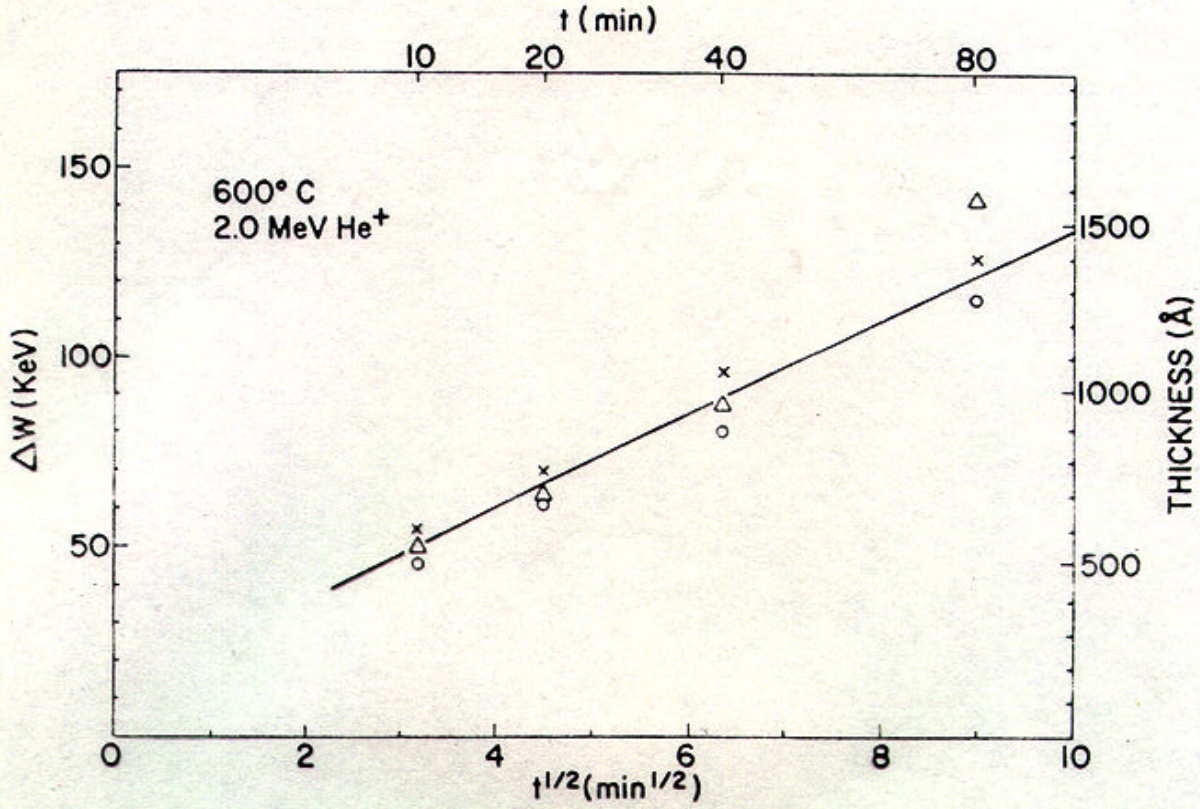


**Figure 9)** The value of ΔW from Figure 8 is plotted against the square root of the heat treatment time, t, for several targets. From this curve we can calculate the diffusion constant of the reaction.

$$\Delta W \sim \sqrt{Dt}$$

$$\Downarrow$$

$$D \sim \left(\frac{\Delta W}{\sqrt{t}}\right)^2$$

Zr verhält sich kinetisch ähnlich wie Hf:

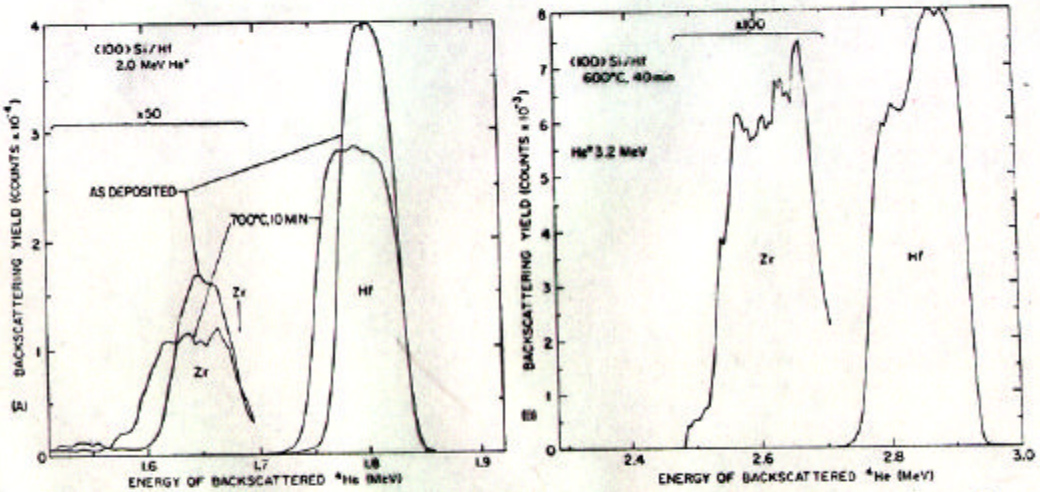


Figure 10| Further analysis of the kinetics of the formation of HfSi is possible by looking at the Zr and Ar peaks (see Figure 4). Shown in the upper part are superimposed spectra of the Hf and Zr peaks in the original target, and after complete formation of the HfSi layer. The Zr peak is diluted in a manner similar to the Hf peak, indicating that they both undergo similar kinetic changes. The lower part shows the HfSi only partly formed, and the Zr peak clearly has a partially diluted peak shape identical to the Hf peak. One explanation is that the Si diffuses through the previously formed HfSi and dilutes the pure Zr and Hf in similar manner in the formation of new HfSi.

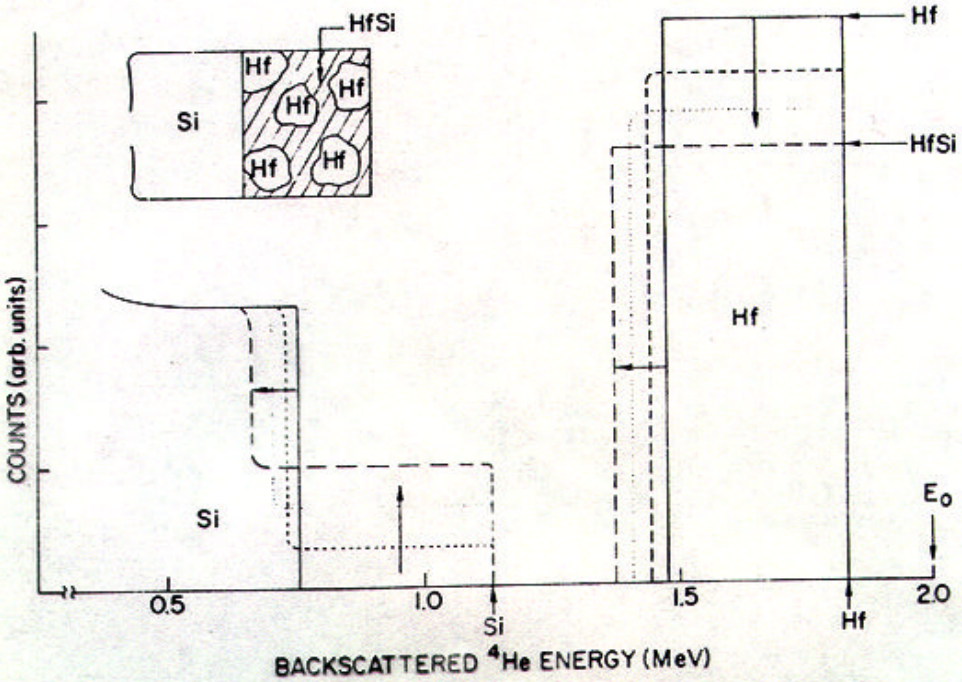


Figure 11) A second possible manner of compound formation is "reaction-limited" (this should be compared to "diffusion-limited" shown in Figure 7). We assume here that the Si diffuses very rapidly along the grain boundaries, but reacts slowly with the Hf grains forming HfSi. The intermediate spectra are different from those of Figure 7, identifying the differences in compound formation kinetics. Note that Si is found all the way at the surface after the shortest heat treatment. Also the Hf peak is immediately diluted in a manner uniform with depth.

Reaktionsbegrenzte Formation einer Verbindung: Diffusion entlang der Korngrenzen ist schnell, aber die Reaktion an den Phasengrenzen ist langsam.

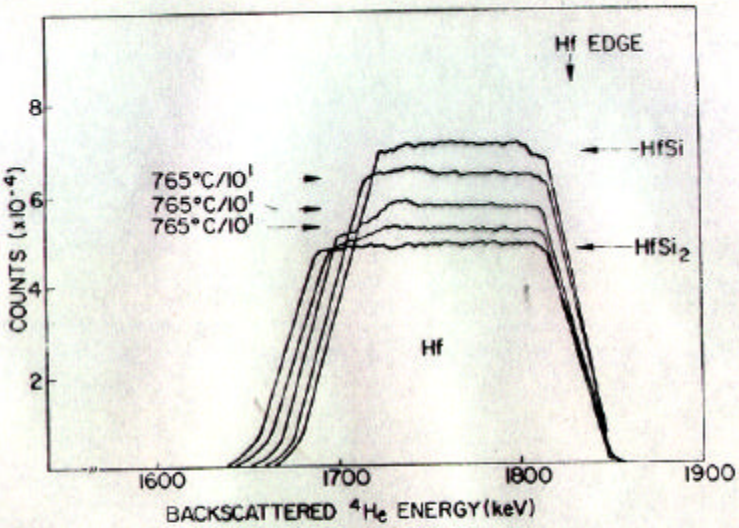


Figure 12) Further heat treatment of the HfSi layer causes the formation of $HfSi_2$. Shown are superimposed spectra of the Hf peak from several samples showing that the intermediate stages of the conversion of HfSi to $HfSi_2$ is similar to the "reaction limited" type described in Figure 11. The fact that all intermediate levels occur with identical heat treatment reflects possibly the sensitivity of the reaction to local stress in the HfSi film. The Si portion of these spectra are similar to the Si peaks illustrated in Figure 11.

# Gegenseitige Diffusion von Ni und Au

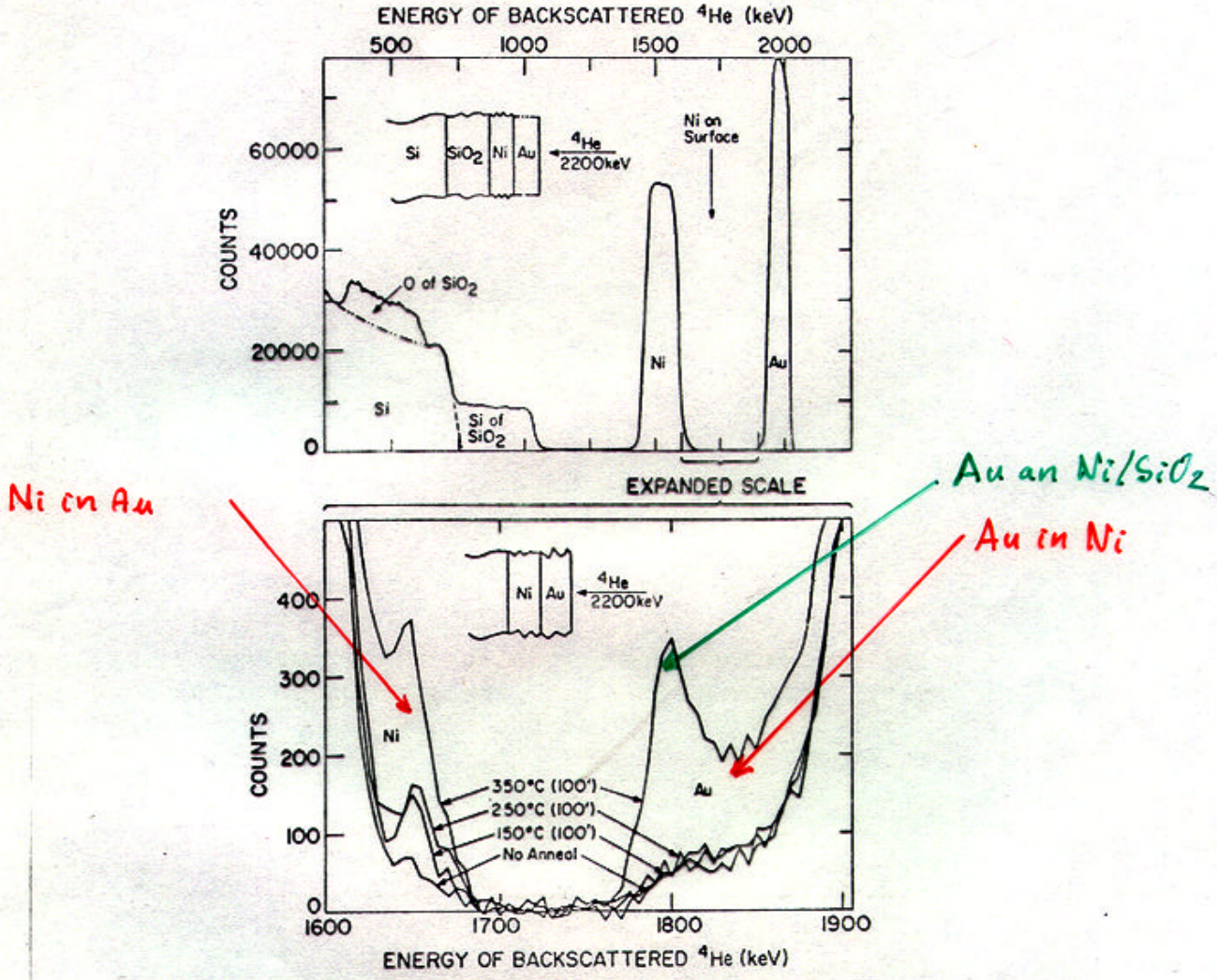


Figure 13) The interdiffusion of two thin metal films is shown for Au and Ni on $SiO_2$. The upper spectrum is from the original target showing the relationship of the various target peaks. Note the Expanded Scale notation (between the Ni and Au peaks) which is shown between the upper and lower drawings. The lower drawing expands this region, and shows superimposed spectra for various heat treated targets. The Ni up-diffusion and the Au down-diffusion are clearly shown.

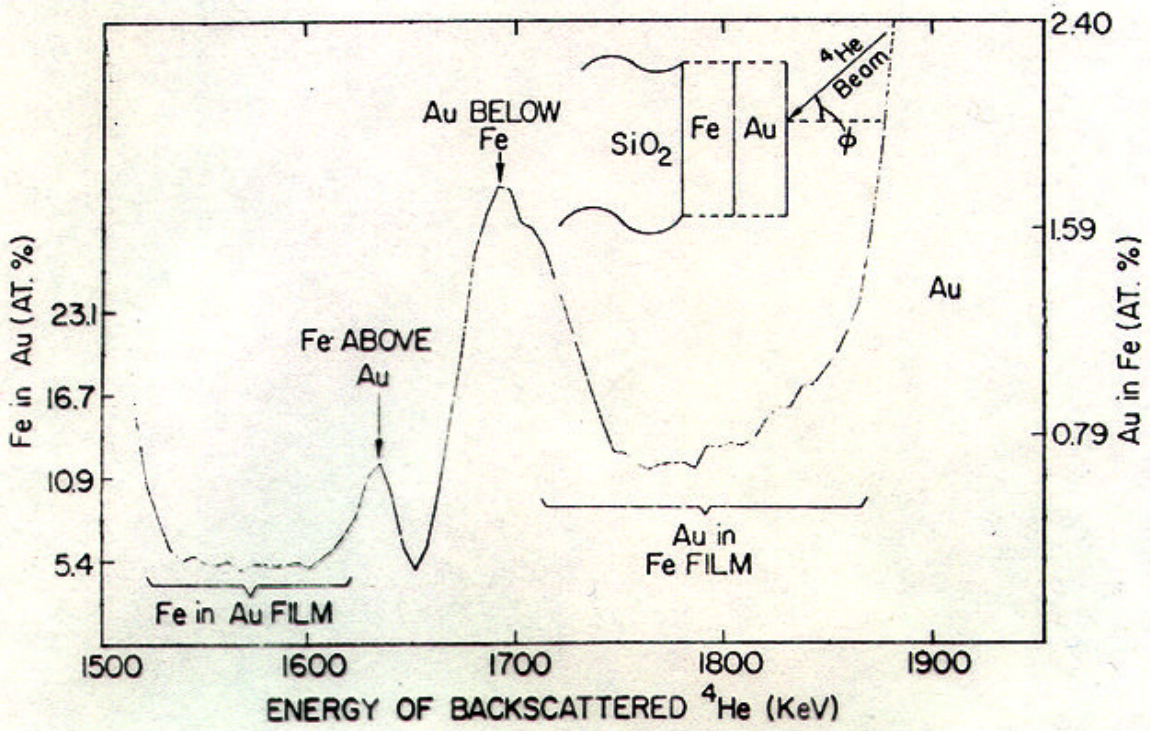


igure 14) By tilting a target of Fe/Au the beam penetrates a hicker target. This expands the region of interest between the two ilms. The ordinate of the spectrum has been converted to atomic ercent of Fe in Au, and Au in Fe, so that concentration profiles an be directly read.

Gedrehte Probe : erhöhtes Auflösungsvermögen für Tiefe

## Eigenschaften der RBS:

- einfach
- quantitativ
- nicht-destruktiv

## Typische Ionen:

$^4He^+$ ($\approx 2\,MeV$)

$^1H^+$ ($\approx 100 \ldots 300\,keV$)

Bei höheren Energien (Coulomb-Schwelle):

Resonanzen.

Bei Protonenenergien $E_p \lesssim 50\,keV$:

Wechselwirkung mit den Elektronen ⇒ neutraler Strahl ⇒ wird nicht nachgewiesen ⇒ verfälscht die quantitative Analyse

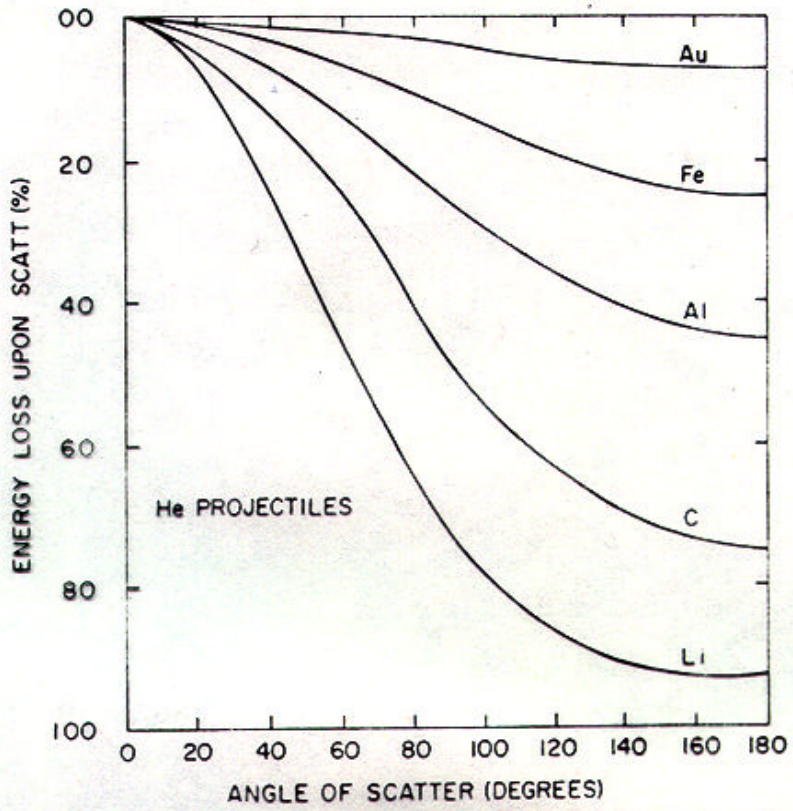


igure 16) Comparison of the recoil energy of $^{4}He$ ions scattering rom various targets at various laboratory angles. In order to eparate elements of similar mass, the scattering should be at a ack angle. This figure is reproduced from Ref. 20.

Gedrehte Probe: schlechteres Auflösungsvermögen für Masse

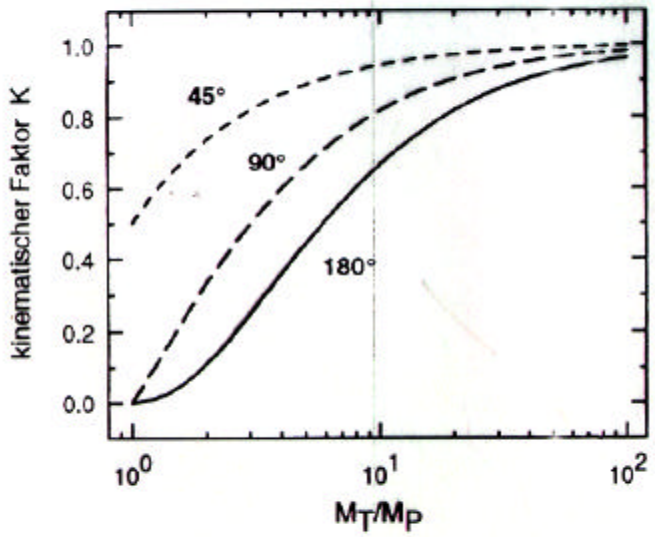


Abb. 11.2
Kinematischer Faktor $K$ als Funktion des Massenverhältnisses $M_T/M_P$ für verschiedene Streuwinkel

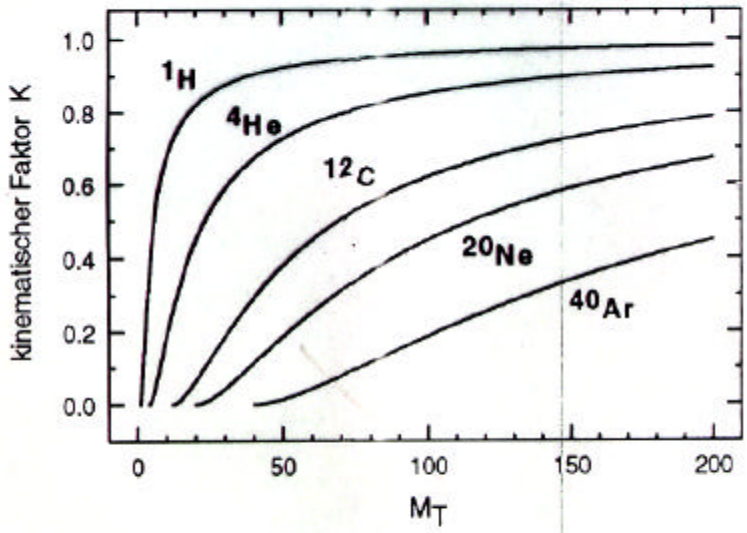


Abb. 11.3 **Kinematischer Faktor für $\theta \approx 170°$** in Abhängigkeit von der Targetmasse $M_T$ für verschiedene Projektile. Für $M_T < M_P$ gibt es keine Rückstreuung

# Ionok fékeződése az anyagban

$$-\frac{dE}{dx} = \frac{4\pi Z_1^2 e^4}{m_e v^2} Z_2 N \left[ \ln \frac{2 m_e v^2}{\langle I \rangle} - \ln\left(1 - \frac{v^2}{c^2}\right) - \frac{v^2}{c^2} \right]$$

$m_e$ : elektrontömeg
$v$ : az ion sebessége

Bethe, Bloch

$$\langle I \rangle \approx 11.5\, Z_2 \ (eV)$$

- $v \ll c \Rightarrow$ a relativisztikus tagok elhanyagolhatók.

$\langle I \rangle \ll E \ll M_2 c^2$ esetén:

$$-\frac{dE}{dx} \approx \frac{1}{v^2} \approx \frac{1}{E}$$

- $E \approx 500 \langle I \rangle$ alatt nem érvényes!
  - kölcsönhatás egyen gén kötött elektronokkal
  - nukleáris (Rutherford-) szórás

Keverékek, vegyületek esetén: súlyozott átlag

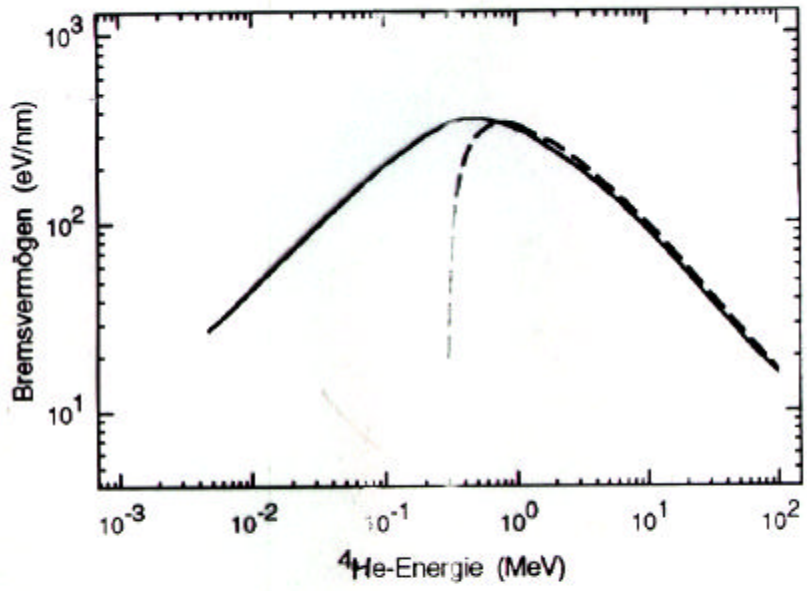


Abb. 11.5 **Bremsvermögen für $^4$He-Projektile** in Silizium als Funktion der Projektilenergie. **Die durchgezogene Linie gibt den Verlauf der experimentellen Daten wieder (ZIE 77). Die gestrichelt Kurve wurde nach Bethe-Bloch** (Gl. (11.10)) berechnet

Im Resonanzbereich (z.B. 3.1 MeV für $^{16}O(\alpha,\alpha)^{16}O$)

kann die Empfindlichkeit für bestimmte

Isotope deutlich erhöht werden.

Auflösungsvermögen für die Masse:

$$\Delta M \sim E$$

$$\Delta M \sim \frac{2m}{(M+m)^2}$$

m: Ionenmasse

M: Targetatom-Masse

⇓

für $m \ll M$ ⇒ großes m günstiger.

Problem: schwere Ionen können energieselektiv kaum nachgewiesen werden.

Praktische Grenzenergien:

200 keV für Protonen

4 MeV für α-Teilchen.

## Wirkungsquerschnitt:

$$\sigma \sim \left(\frac{Z_1}{E}\right)^2$$

Für Oberflächenverunreinigungen aus schweren Elementen an leichten Substraten sind schwere Ionen ($^{12}C$, $^{16}O$, u.s.w.) gut geeignet.

Für leichte Ionen (z.B. $^4He^+$) muß die Energie reduziert werden, damit eine höhere Effektivität erreicht wird, aber $\Rightarrow$ schlechtere Energie-auflösung.

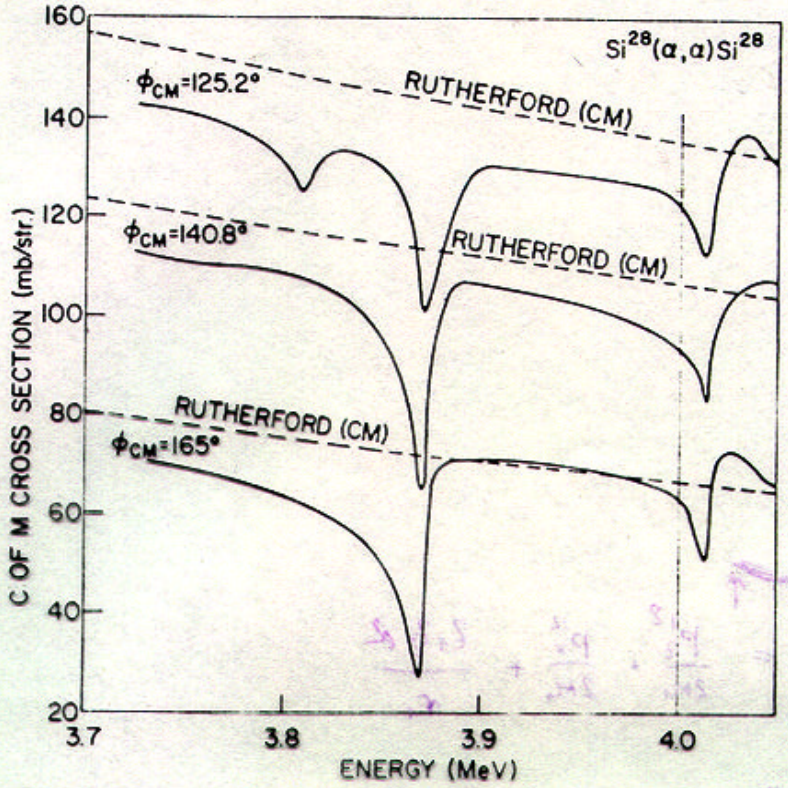


Figure 15) Comparison of $Si^{28}$ ($^4He$, $^4He$) $Si^{28}$ experimental elastic cross sections to Rutherford cross-sections (including recoil terms) for several angles. All angles and cross-sections are in center-of-mass coordinates. Actual data points were in steps of 2.5 keV and were replaced by smooth curves. This data was supplied by McEllistrem and Leung (Ref. 19) who are conducting a complete low energy analysis of this reaction.

Die ersten Resonanzen der Streuung

$^{28}Si\ (\alpha, \alpha)\ ^{28}Si$